Available online at www.sciencedirect.com

SciVerse ScienceDirect

Ceramics International 38 (2012) 5165–5173

CERAMICS INTERNATIONAL

www.elsevier.com/locate/ceramint

Development of novel carbon bonded filter compositions for steel melt filtration

Marcus Emmel *, Christos G. Aneziris

Technical University Bergakademie Freiberg, Institute of Ceramic, Glass- and Construction Materials, Agricolastraße 17, 09599 Freiberg, Germany

Received 17 October 2011; received in revised form 6 March 2012; accepted 7 March 2012
Available online 16 March 2012

Abstract

Carbon-bonded alumina filters for steel melt filtration are increasingly used by steel foundries. Their potential regarding material characteristics and filtration efficiency has not been fully exploited yet. A new filter composition based on the synthetic coal tar pitch Carbores® P, has been explored. Its compatibility with a water-based dispersing system allows additions of carbon black, graphite, and additives to reach a residual carbon content of up to 30 wt.%. For determining physical properties and variables of the respective compositions, 10 pores per inch (ppi) foam ceramic filters were manufactured via the Schwartzwalder process. The influence of different binder contents on the processing properties and mechanical characteristics of the system was evaluated. Based on these studies, an increase in cold crushing strength of approx. 30% has been achieved in comparison to current state of the art materials.

Keywords: D: Al_2O_3; D: Carbon; E: Refractories; Ceramic foam filter

1. Introduction

In order to remove oxide inclusions and ensure the requirements of high purity metal castings, ceramic foam filters have been used in steel applications for several years. Foam filters are exposed to casting temperatures between 1400 and 1650 °C for approx. 30 s per ton of cast steel [1]. The portion of inclusions, their kind, form, and distribution are of great importance for influencing material properties in applications such as high-tensile steels. They determine to a large extent the deformation and breaking behavior, as well as the physical properties of the steel. During load, stress concentrations are generated in the proximity of inclusions [2,3].

Difficulties primarily appear during the verification of inclusions in aluminum-deoxidized steel, especially in the distinction between primary, secondary and tertiary inclusions [4]. The notched bar impact strength of a material characterizes its resistance against crack initiation and growth. The negative influence of different inclusions is represented by the time of their formation in the notched-bar impact-strength of steel samples. The observation of inclusions in aluminum deoxidized iron has been examined by Wasai et al. [5], who assigned the dendritic, maple-like and polygonal inclusions to the group of primary inclusions. These flaws consist of alumina, with some having small quantities of iron or silicon and aluminum present. In contrast, the network-like, coral-like, and spherical inclusions; which are composed of alumina, hercynite and wüstite; were classified as secondary inclusions. Regarding the secondary inclusion-alumina, α-, γ-, and δ-structures were detected. Moreover, amorphous silica inclusions could be observed.

Janke et al. and Hammerschmid discussed filtration mechanisms, filtration efficiencies, filter materials, and filter structures for steel melts [1,6,7]. According to Dávila-Maldonado et al. [8] the filtration efficiency of ceramic foam filters of non-metallic inclusions in ferrous melts is less than 75% in the particle size range from 1 to 100 μm. Concerning the thermo mechanical requirements of filter materials and filter structures; thermal shock resistance, refractoriness under load, and sufficient mechanical strength at temperatures > 1480 °C for the iron casting process are necessary with respect to ecological as well as economical demands nowadays.

The different types of ceramic filters include foam filters, extruded cellular ceramic filters, and pressed filter cores [9].

* Corresponding author.
E-mail address: Marcus.Emmel@ikgb.tu-freiberg.de (M. Emmel).

0272-8842/$36.00
doi:10.1016/j.ceramint.2012.03.022

The production technology for ceramic filters with defined porosity for the molten bath filtration, using a pressing technique, was investigated by Mogilevskii [10]. The filters he evaluated had a macro porosity of 70% and macro pore sizes from 1 to 5 mm, and were studied regarding their permeability for metal melts at temperatures above 1450 °C. The filters were pre-heated up to 900 °C before application.

Adjustment of the metal flow and its transformation from a turbulent into a laminar flow are further functions of ceramic foam filters. With a turbulence-free flow, the risk of reoxidation of the metal and the formation of cavities is minimized, resulting in improvement of surface quality and shorter casting times [11]. More information regarding other filter structures, as well as their production processes, are described by Luyten et al., who discuss manufacturing techniques such as gel casting, a hollow beads method, and a reaction-bonded modified polyurethane technique [12].

In the present work, the replica technique patented by Schwartzwalder in 1963 was used [13]. State of the art polyurethane (PU) foams serve as a template for the replica technique, with a 10 pores per inch (ppi) macrostructure for steel applications and 30 ppi for aluminum melts. During the thermal treatment, the PU foam softens and volatilizes [14]. The foams represent a negative of the desired final structure of the ceramic filter, and are composed primarily of open cells with a pentagon-dodecahedronal geometry linked by triconcave struts. After the foam structure is burned out, the hollow ceramic struts have sharp edges, which generate critical stress concentrations, and consequently can lead to severe loss of strength [15]. Regarding the thermo mechanical requirements with respect to optimal casting temperatures, by avoiding metal melt freezing, an optimum wall thickness of approximately 0.3 mm is required [16,17].

In comparison to other materials, carbon has an extremely high refractoriness, and is characterized by high thermal conductivity, resulting in high thermal shock resistance. Carbon also presents higher cold crushing strength (CCS) with increasing temperature (up to 2500 °C) owing to the annealing of cracks and structural-related errors [18]. It is commonly known that carbon containing materials show improved creep resistance [16]. According to Stephani et al., the pseudoplastic behavior of carbon in the Al_2O_3–C system leads to less influence of the density and cell size of the cellular structure on the mechanical properties of the filters. As a result of the short casting times and the low wettability of carbon, Al_2O_3–C-filters do not have an increased pick-up of carbon in the filtrated steel. [19]

For the generation of the carbon-bonds, which serve as a matrix bond between the alumina particles, pitches and resins are predominantly used in the refractory industry. In terms of this contribution, the solid coal tar pitch Carbores® P (Carbonacious Resin), which has already been used in manufacturing of carbon bonded MgO–C bricks [21], with a benzo(a)pyren content of <500 ppm, was used as bonding agent as well as a carbon source for filter production [20]. The newly developed and characterized compositions of the present work offer innovative approaches for the manufacturing of carbon-bonded filter materials since the established binder system for carbon bonded filters based on Rauxolit® (Rütgers, Germany) is no longer produced. As a consequence of its low volatile content, the carcinogenic effect of Carbores® P is negligible compared to other pitches (Carbores® P has approximately 3% of the toxic potential of usual pitches). It is also characterized by a softening point higher than 200 °C, and a residual carbon content up to 85%. By means of heat treatment, the volatile components of Carbores® P are removed, and a graphitization process of the pitch is achieved through the formation of an intermediate pitch-mesophase compound [22,23]. The softening of the pitch during the thermal treatment, its easy dispersion in water, and a high residual carbon that forms a high amount of crystalline material after pyrolysis at temperatures below 1000 °C provide major advantages in manufacturing of carbon-bonded filter structures.

2. Materials and methods

The raw materials used for the preparation of the investigated Al_2O_3-C compositions were alumina (Martoxid MR 70, Martinswerk, Germany, 99.80 wt.% Al_2O_3, $d_{90} \leq 3.0$ μm), modified coal tar pitch powder (Carbores® P, Rütgers, Germany, $d_{90} < 0.2$ mm – used as a binder as well as a carbon source), fine natural graphite (AF 96/97, Graphit Kropfmühl, Germany, 96.7 wt.% carbon, 99.8 wt.% <40 μm), carbon black powder (Luvomaxx N-991, Lehmann & Voss & Co., Germany, ≥99.0 wt.% carbon, >0.01 wt.% ash content, primary particle size of 200–500 nm), and a submicron silica (SUBMICRONSILICA 995 U, Elkem, Norway, ≥99.5 wt.% SiO_2, 100 wt.% <0.4 μm). The additives were polypropylene glycol (PPG P400, Sigma–Aldrich, Germany – used as a wetting agent), ligninsulfonate (T11B, Otto-Dille, Germany – used as a temporary binder), Castament VP 95 L (BASF, Germany – used as a dispersing agent), and Contraspum K 1012 (Zschimmer & Schwarz, Germany – used as an antifoam agent).

The carbon-bonded filters were manufactured in two steps. First, a highly viscous impregnating slurry was prepared in a high shear Hobbart-type mixer (ToniTechnik, Germany). In the beginning, the respective powder mixtures listed in Table 1 were dry mixed for 5 min in a Hobbart-type mixer. After this step, the additives were dispersed in deionized water and then added to the powder mixture, followed by further additions of deionized water until a plastic mass was formed. This mass was kneaded for additional 5 min. This led to better homogenization, and destroyed any agglomerates by shear force. Further additions of deionized water were made while measuring the viscosity (by means of a hand viscometer Haake, Germany) until a value of approximately 600 mPa s was obtained.

The resulting slurry was subsequently used to impregnate PU-foam blocks (50 mm × 50 mm × 20 mm). The slurry was hand-pressed into the PU-foam to ensure a complete coating of the polyurethane skeleton. In order to create the first coating on the polyurethane skeleton, it was necessary to remove excess impregnation slurry. Therefore each PU-foam block (filled with slurry) was pressed through a roll-pressing device that consisted

Table 1
Composition of the investigated samples, including the total solid content of the impregnating slurry, the spraying slurry, and the additives.

	1	2	3	4	5	6	7	8	9
Al_2O_3 Martoxid MR 70 [%]	68	67	66	61	65	64	64	64	64
Carbores® P	10	15	20	20	25	30	30	30	30
Graphite AF 96/97	12	10	8	8	5.5	3.3	3.3	6	–
Carbon black MT N-991	10	8	6	6	4.5	2.7	2.7	–	**6**
Submicron silica 995	–	–	–	5	–	–	–	–	–
Additives [%][a]									
Lignin sulfonate T11B	1.5	1.5	1.5	1.5	1.5	1.5	1.5	1.5	1.5
PPG P400	0.8	0.8	0.8	0.8	0.8	0.8	0.0	0.8	0.8
Castament VP 95 L	0.3	0.3	0.3	0.3	0.3	0.3	0.3	0.3	0.3
Contraspum K 1012	0.1	0.1	0.1	0.1	0.1	0.1	0.1	0.1	0.1
Total solid content [%][b]									
Impregnating slurry	81.67	82.32	83.01	77.20	84.41	85.69	85.69	85.69	85.69
Spraying slurry	74.14	75.57	76.05	70.86	77.41	79.14	79.14	79.14	79.14

[a] Related to solid.
[b] Including the alumina, the carbon sources, and the silica (without additives).

of two counter rotating rolls with a diameter of 44 mm. The gap between the rolls was 4 mm and the rotation speed of them was 60 revolutions/min. Subsequently, the impregnated foams were dried for 12 h at 25 or 40 °C to a constant weight. During this process step, the generation of unfavorable defects due to the relaxation of the squeezed foam and drying were observed in the filters. Note that the desired thickness of the ceramic coating was not easily adjusted under normal processing conditions. Thus, a further step – the spraying of a second ceramic layer – had to be accomplished.

Spraying of the dried foams was carried out in a spraying chamber. A spray gun SATAjet B (Sata, Germany), with a nozzle diameter of 1.4 mm and a spraying pressure of 3 bar was used. The distance between the nozzle and filter was kept constant at approximately 10 cm. The spraying took place on all 6 sides of the filter. The largest sides, in regard to the surface area, were sprayed for 3 s; and the smaller dimensioned sides, for about 1 s, resulting in a wet filter weight of 25 g. The sprayed samples were subsequently dried again at 25 °C or 40 °C, for 12 h and reweighed.

The dried filter was thermally treated by a pyrolysis process, shown in Fig. 1, which took place in retorts filled with calcined petcoke (Müco, Germany) having a particle size between 0.2 and 2.0 mm. The final temperature of 800 °C was reached with a heating rate of 1 K/min and a holding time of 180 min. Additional holding time steps of 30 min were adopted every 100 °C, after which the samples being thermally treated were allowed to cool down inside the oven.

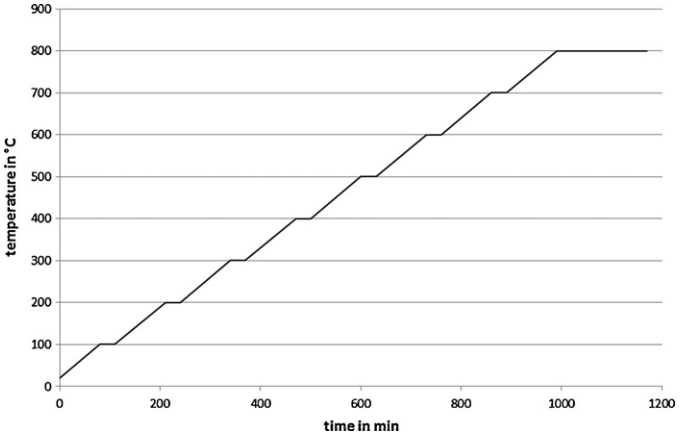

Fig. 1. Heating rate schedule for the thermal treatment of the samples.

2.1. Rheology

The rheological behavior of the slurries was measured using a rheometer RheoStress RS 150 (Haake, Germany). For the measurement of the flow curves, a coaxial cylinder measuring system of the type 01038 Z40 DIN Ti was used. The flow behavior was determined by measuring the viscosity and shear stress during variations of the shear rate. This was changed linearly from 0.1 to 1000 s^{-1}, and was kept at this level for 90 s before it was reduced with the same rate to the initial 0.1 s^{-1} value. The 1000 s^{-1} is cited as a common value achieved during the spray process [24].

2.2. SEM

A Philips XL 30 (Philips, Germany) scanning electron microscope was used for evaluation of the microstructure changes.

2.3. Open porosity

Open porosity was determined using a mercury porosimeter (PASCAL series, Porotec, Germany).

2.4. Carbon content

In order to verify direct influences of different parameters on the total carbon content and on the varying carbon sources, qualitative and quantitative determinations were measured using two analysis methods.

A RC 412 (Leco, USA) carbon analyzer was used for both the qualitative and quantitative analyses of the carbon content. About 20 mg of the sample material was ground for 2 min in a

disk oscillating mill, than burned in an oxidizing atmosphere, producing CO_2 from the carbon. A firing curve from 150 to 900 °C with a heating rate of 50 K/min was selected for the carbon analysis. The carbon measurement is based on the different infrared adsorptions with changing temperature, permitting conclusions on the respective carbon source types.

With the aid of the carbon analyzer type ''vario MICRO cube'' (Elementar, Germany), the samples were examined according to their quantitative carbon content. For these measurements the samples had to be ground using a mortar and pestle to guarantee a certain particle size and homogenous samples. For the measurement, approximately 2 mg of the material were weighed in tin caps and burned at 1150 °C in an oxidizing atmosphere. The change in thermal conductivity of the gas was detected, and from this the total carbon content was calculated.

2.5. CCS

The cold crushing strength (CCS) was determined on a universal testing machine TT 2420 (TIRA GmbH, Germany) using a 20 kN pressure cell. The displacement speed was 3 mm/min until a counteracting force of 5 N was reached. At this load, the displacement speed was changed to 1 N/mm^2/s. The experiment was terminated when a strength loss of 80% was reached.

2.6. Computer tomography

In order to detect the strut thickness distribution, foams were analyzed using a Micro focus X-ray computer tomograph CT-ALPHA (ProCon X-Ray, Germany) equipped with a 160 kV X-ray source and a C7942SK-05 (Hamamatsu, Japan) detector with 2024 × 2024 active pixels. Measurements were made at 155 kV, and the received cubic pixel (voxel) had a size of 65 μm × 65 μm × 65 μm.

3. Results and discussion

3.1. Rheological behavior

Pure Carbores® P had a shear thickening and thixotropic behavior as shown in Fig. 2. It is clearly visible that a minimum amount of carbon black and graphite are required for the generation of a stable and shear thinning slurry. The effect of those additions causes the changes of the manufacturing properties of the spraying slurries, illustrated in Fig. 3. Due the higher packing density, the addition of both graphite and carbon black into the mixture causes increased viscosity values of about 86 mPa s, whereas a pure addition of graphite or carbon black decreases the viscosity to a value of 65 mPa s. Graphite exhibits a flaky structure that means the particles can slide along each other. Using Carbores® P leads to increased catching of the strongly structured particles with rising shear rate due to its grain morphology (Fig. 4). The addition of black carbon or graphite (Fig. 3) results in a shear thinning behavior. The addition of

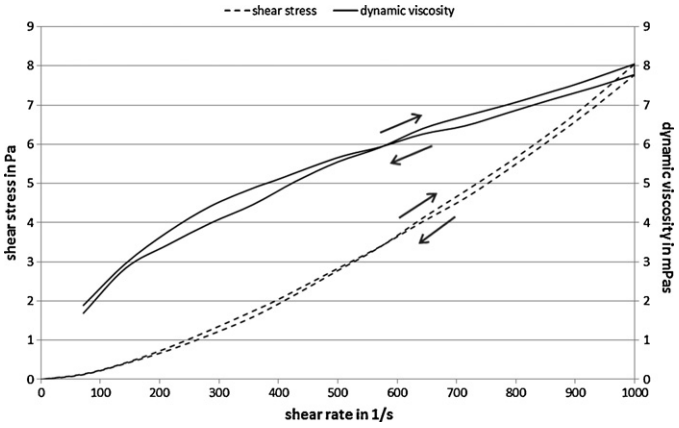

Fig. 2. Rheological behavior of dispersed Carbores® P.

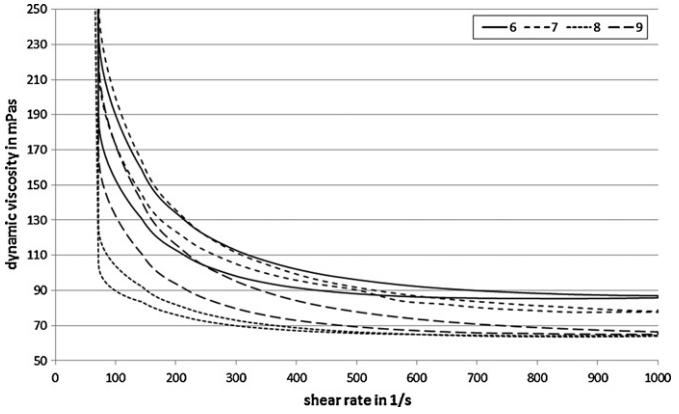

Fig. 3. Rheological behavior of spraying slurries, based on mixtures 6–9, as listed in Table 1.

polypropylene glycol (PPG P400), which acts as a wetting agent, causes an increase of the dynamic viscosity. The viscosities of the impregnating slurries, tested at a shear rate of 200 1/s, show values higher than 600 mPa s.

3.2. Total solid content with respect to the Carbores® P content

The total solid content for samples; including the alumina and the carbon sources for compositions number 1, 2, 3, 5, and 6; is shown in Fig. 5. It is noted in this figure that the water requirement decreases with increasing Carbores® P content. This is caused by the different specific surface areas of the powder raw materials.

Martoxid MR 70 has a BET-surface area of approximately 8 m^2/g, graphite of approximately 12 m^2/g, and the carbon black is assumed to have a large BET-surface due to its small particle size when compared to Carbores® P, which has a specific surface area of about 0.6 m^2/g. The partial substitution of alumina, graphite, and carbon black with the Carbores® P results in a lower water requirement with the same viscosity. Thus it is possible to increase the solid content of the impregnating slurries from 81.67 wt.% to 85.69 wt.%.

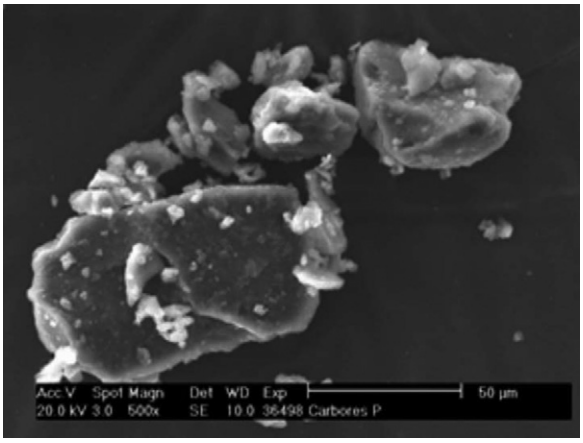

Fig. 4. Grain morphology of Carbores® P.

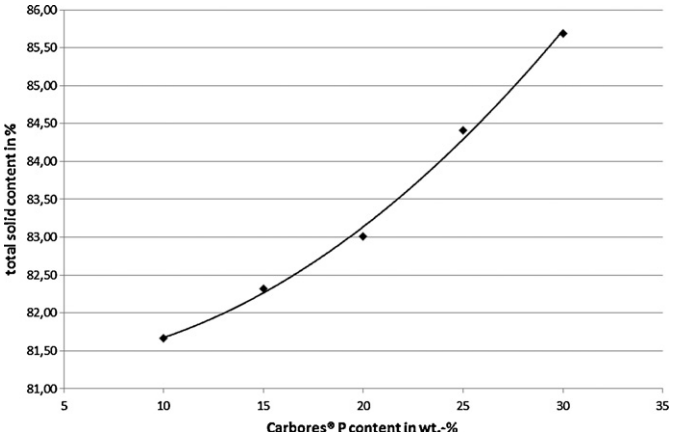

Fig. 5. Total solid content with respect to the Carbores® P content, based on mixtures 1, 2, 3, 5, 6, as listed in Table 1.

3.3. Stages of the pyrolysis

Different stages of the thermal treatment of filters are illustrated in Fig. 6. Volatilization of organic components out of the binder occurs at approximately 200 °C. At a temperature of 400 °C, the pyrolysis of the PU-foam is complete and the appearance of mesophase (a phase intermediate between solid and liquid) caused by Carbores® P occurs. This mesophase turns into the solid state between 500 and 550 °C, followed by the dehydration of volatile components, which contributes to sample shrinkage up to the final temperature.

3.4. Residual carbon content with respect to the Al_2O_3 content

By using a carbon analyzer (Leco, USA), different kinds of carbon could be detected qualitatively. Regarding the quantitative determination of the carbon content using this method, however, a high statistical spread resulted with poor curve reproducibility, preventing meaningful conclusions. The use of the micro elementary analyzer, however, led to reproducible measured values of the residual carbon content. Although a qualitative phase separation was not possible, accuracy of this procedure let to its use. It was found that Al_2O_3 has a significant influence on the carbon yield (Fig. 7) for compositions number 1, 3, 4, and 6. That means the smaller the oxide content, the higher the generation of residual carbon. This is traceable back to the function of the alumina as an electron acceptor, which was described similarly by Yamaguchi et al. [25]. According to Yamaguchi, an improvement of the carbon yield could be obtained with the same carbon amount in the basic composition by a partial substitution of alumina by SiO_2, which has an ability to donate electrons. During the coexistence of SiO_2 and graphite, the SiO_2 donates electrons to graphite, which leads to a favored electron distribution, and thus to an inhibition of graphite oxidation. Regarding the addition of the SiO_2, an increase of the carbon yield could be generated, as well as an increased standard deviation and a reduction of the total solid content. Due to the very large specific surface area, an increase of the water requirement resulted from the SiO_2 additions, which leads to more drying cracks.

3.5. Residual carbon content with respect to the carbon source and additive variation

From Table 2, it is clear that a decrease of the residual carbon content results from the addition of PPG P400. Regarding the influence of graphite and carbon black, it is noted that the addition of pure graphite provides higher carbon yields compared to the carbon black containing mixtures. This is caused by the different particle sizes, which exert a direct influence on oxidation resistance. In the case of graphite, which has a hexagonal structure and larger grain sizes than carbon black, the oxidation resistance is increased. In contrast, the carbon black has considerably smaller grain sizes, more

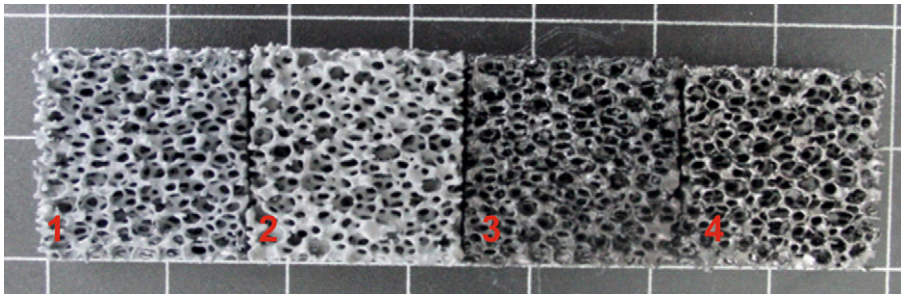

Fig. 6. Stages of the pyrolysis at room temperature (1), 200 °C (2), 400 °C (3), 800 °C (4).

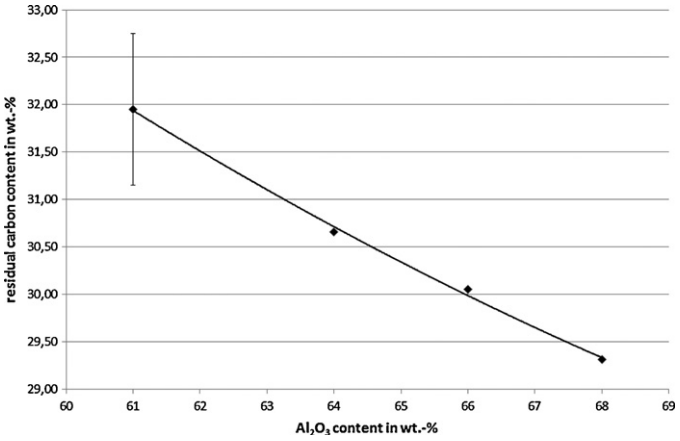

Fig. 7. Residual carbon content with respect to the Al_2O_3 content, based on mixtures 1, 3, 4, 6, as listed in Table 1.

Table 2
Residual carbon content, and cold crushing strength with respect to the carbon source and additive variation, based on mixtures 6–9, as listed in Table 1.

Sample	6	7	8	9
Residual carbon content in %	30.42	31.43	31.08	29.54
Standard deviation in %	0.11	0.30	0.18	0.27
CCS in N/mm^2	0.50	0.62	0.42	0.41
Standard deviation in N/mm^2	0.14	0.10	0.15	0.20

defects, weaker C–C bonds, and does not exhibit a highly crystalline structure. This leads to a greater reactive surface area, which reduces the oxidation resistance of carbon black, although it shows a higher carbon content.

3.6. Volumetric shrinkage with respect to the Carbores® P content

The volumetric shrinkage increases with increasing Carbores® P content and decreasing alumina content. On the one hand, volatile components are given off both from the organics like the PU-foam and the Carbores® P, and from adsorbed gases and water vapor of the carbon black, due to the thermal treatment. The alumina contains no volatiles, causing it to counteract the volumetric shrinkage with increasing content. Although the amount of adsorbed gases and water vapor arising from the carbon black and the graphite are reduced as a consequence of the Carbores® P addition, the volumetric shrinkage increases. With an increasing content of the bonding agent (Carbores® P), the proportional of volatile components are increased, which affects the shrinkage behavior. The second factor of influence is based on Carbores® P and the occurrence of a liquid carbon containing phase at temperatures $> 200\ ^\circ$C, which intensifies the volumetric shrinkage. Fig. 8 shows a higher quantity of liquid phase due to the higher Carbores® P content.

The pyrolysis of the coal tar pitch is connected with graphitization, and leads therefore to a shrinkage afflicted alignment of the graphitic structures. It is noted that the Carbores® P content has an essential influence on volumetric shrinkage, causing it to increase with increasing content due to the appearance of the liquid phase, and to its high amount of volatiles, compared to that of carbon black, and graphite. So a volume shrinkage is measured at 2.3%, according to Fig. 9, with a bonding agent content of 10 wt.%, whereas a Carbores® P content of 30 wt.% increases the volume shrinkage up to 8.2%.

3.7. Open porosity with respect to the Carbores® P content

Fig. 10 shows the open porosity variations with respect to the Carbores® P content. The decreasing porosity is in part caused by the increasing total solid content, which reduces pore formation. In addition, the increasing residual carbon content counteracts an elevated porosity. Besides the increasing volumetric shrinkage, the occurrence of a liquid phase due to the thermal treatment of Carbores® P influences the porosity of the samples number 1, 2, 3, 5, and 6. This liquid phase infiltrates pores and leads to a porosity decrease with respect to the increasing Carbores® P content. Thus the influence of the liquid phase on the porosity is more pronounced, compared to the volatiles, given off from the binder, carbon black, graphite, and the PU-foam.

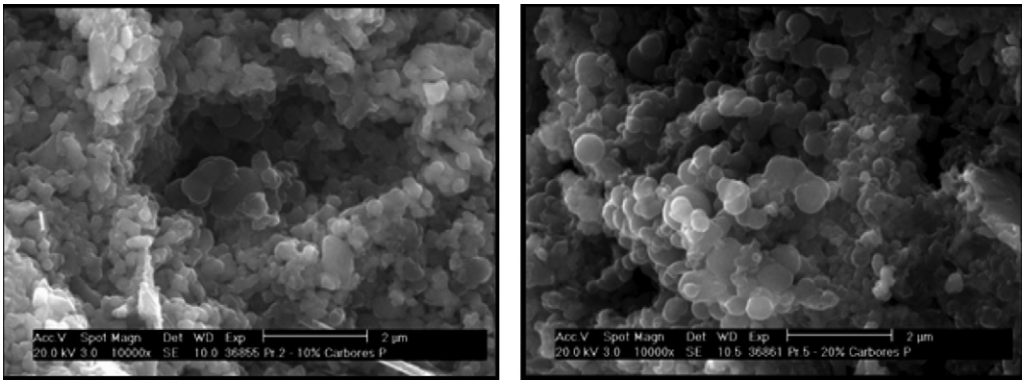

Fig. 8. SEM image of filter with 10 wt.% Carbores® P (left, mixture 1 as listed in Table 1) and 20 wt.% Carbores® P (right, mixture 2 as listed in Table 1), after pyrolysis at 800 °C.

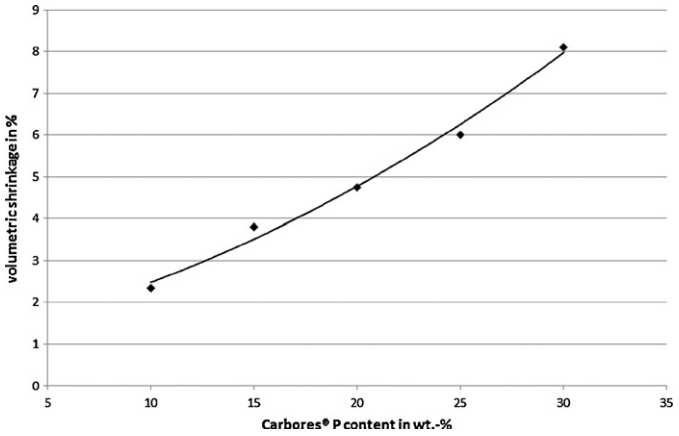

Fig. 9. Volumetric shrinkage in respect to the Carbores® P content, based on mixtures 1, 2, 3, 5, 6, as listed in Table 1.

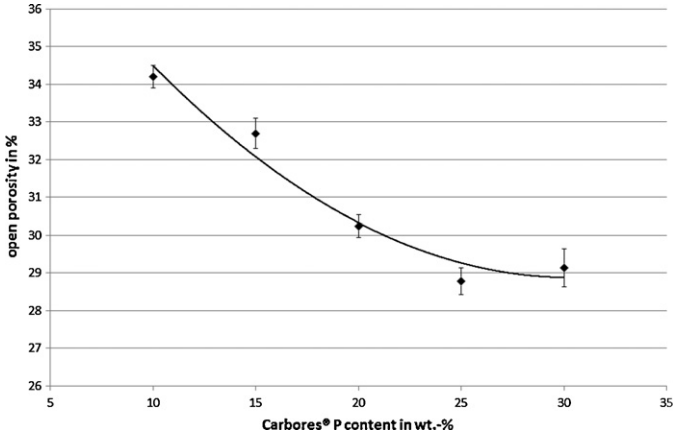

Fig. 10. Open porosity with respect to the Carbores® P content, based on mixtures 1, 2, 3, 5, 6, as listed in Table 1.

3.8. Cold crushing strength with respect to the weight

In order to determine the influence of the filter weight on the cold crushing strength of the filter systems, samples with different weights of the same composition, due to varying spraying times, were tested. The weight of the filters in the pyrolysed condition varied from 17.2 g to 20.7 g. As evident from Fig. 11, the CCS increases with increasing filter weight. Thus, the filters of 17.2 g exhibit a CCS of about 0.03 N/mm^2, which can be increased up to 0.1 N/mm^2 for the filters with a weight of 20.7 g. That means that the CCS increased by approximately 3 times for a 20 wt.% increase in sample weight. Filter weight can be used as an indicator of sample strength, and highlights the importance of strut thicknesses. A high mass content means an increase of strut thicknesses, which leads to

Table 3
Cold crushing strength with respect to the drying temperature, based on mixture 6, as listed in Table 1.

Drying temperature in °C	25	40
CCS in N/mm^2	0.50	0.26
Standard deviation in N/mm^2	0.14	0.06

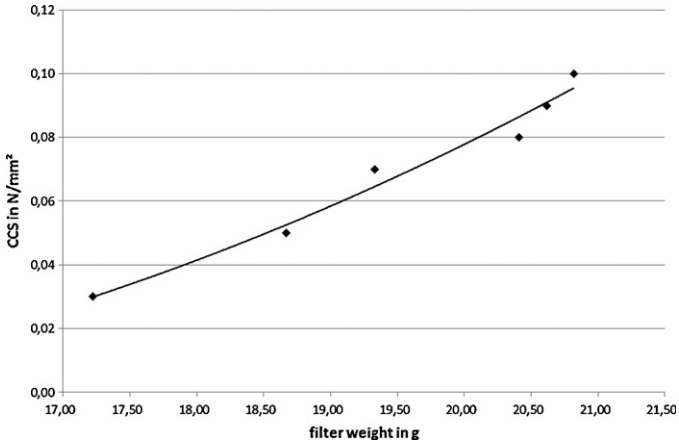

Fig. 11. Cold crushing strength with respect to the weight, based on mixture 1, as listed in Table 1.

an increase in sample cross section, and of CCS. In order to generate meaningful results regarding the influence of the Carbores® P, the masses must be kept constant.

3.9. Cold crushing strength with respect to the drying temperature

The influence of drying temperature on CCS after pyrolysis at 800 °C is presented in Table 3. The evaporation of water within the filter struts results in lower CCS at 40 °C versus 25 °C. Micro-cracks result at 40 °C, which do not heal completely during pyrolysis, versus drying at 25 °C, where micro-cracks were not found, and is thought to be the cause of the higher CCS at that temperature.

3.10. Cold crushing strength with respect to the carbon source and additive variation

The results of CCS with respect to the carbon source and additive variation (Table 2) correlate with these of the residual carbon content, also shown in Table 2 and discussed in Section 3.5. From this it follows that with decreasing residual carbon content, the CCS decreases as well. The reason for this is the

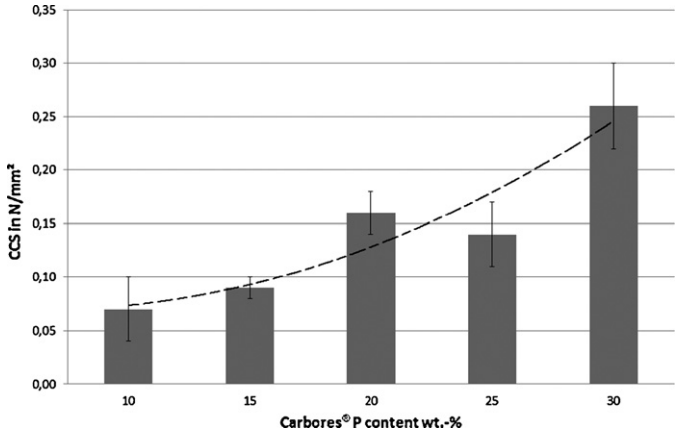

Fig. 12. Cold crushing strength with respect to the Carbores® P content, based on mixtures 1, 2, 3, 5, 6, as listed in Table 1.

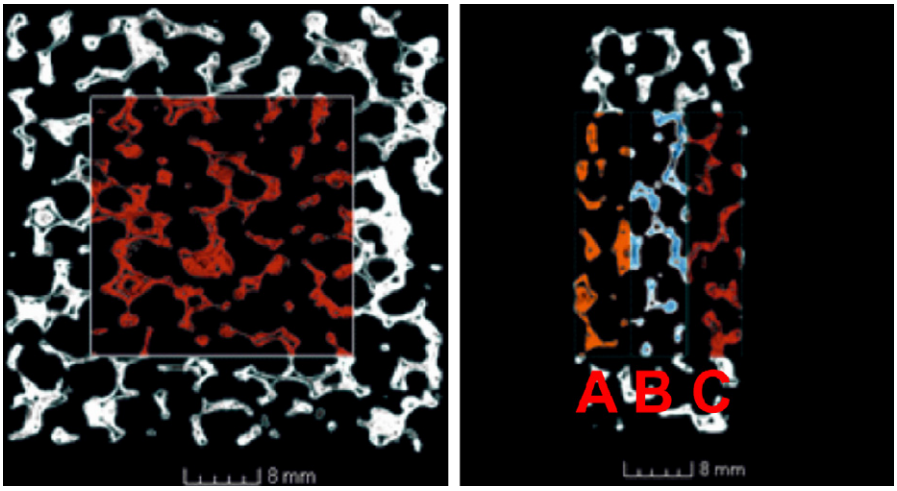

Fig. 13. Filter sections for the investigation of strut thickness distribution (left image: top view; right image: side view, including the sections A–C).

reduction of the binder amount. The difference between the CCS of the graphite and the carbon black free mixtures are less pronounced compared to the difference in the carbon yield. This is thought to be due to the higher strength of carbon black. The only exception with this relationship is if the mixture containing both graphite and carbon black, which have a comparatively higher CCS. Due to the varying grain sizes of the carbon sources, the packing density increases, resulting in a higher CCS.

3.11. Cold crushing strength with respect to the Carbores® P content

As noted in Fig. 12, a relationship exists between CCS and Carbores® P as a bonding agent. Increased additions of Carbores® P, in combination with an increased residual carbon content, lead to an improved degree of cross-linking of the particles among themselves, and thus to stronger bonding. It was noted that greater shrinkage at high Carbores® P levels caused fewer cracks, helping to increase CCS. The infiltration of pores with the liquid phase also decreases the total porosity, leading to higher CCS, which was approximately four times greater than at lower Carbores® P additions.

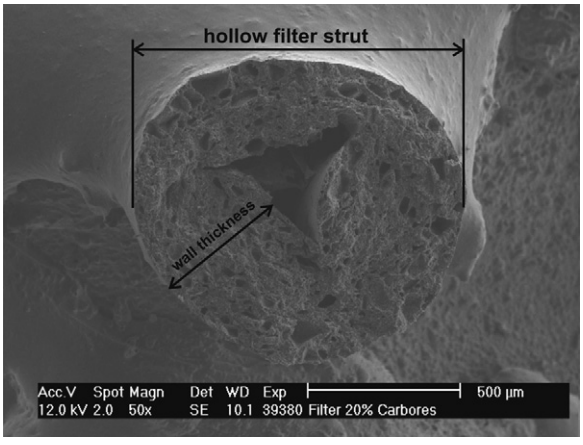

Fig. 14. Cross section of a filter strut, with 20 wt.% Carbores® P, after pyrolysis at 800 °C.

3.12. Computer tomographical investigation of the wall thickness distribution

Results regarding the wall thickness distribution conducted with the aid of the computer tomography were determined within the sections shown in Fig. 13. The tested filters exhibit, irrespective of varying mixtures, the same characteristics. The sections A and C consist of a wall thickness distribution of approximately 400 μm (±230 μm). In contrast, section B, which is located in the middle of the filter, had wall thicknesses of about 300 μm (±160 μm). Fig. 14 illustrates a fractured section of a filter strut including the wall thicknesses. Due to the shear thinning behavior, the viscosity of the respective slurries increases immediately after striking the impregnated filter struts. Therefore the slurry entry into the filter interior is reduced, which is intensified by the resistance to slurry flow that increases with increasing filter depth, resulting in thinner struts.

4. Conclusions

The development of filter materials and filter structures for steel melt filtration, based on the synthetic coal tar pitch Carbores® P as a binder as well as a carbon source, was achieved in the present work. The requirement of a shear thinning slurry system was obtained in filters containing both graphite and carbon black. Moreover the influences of both the graphite and carbon black in terms of the cold crushing strength and the residual carbon content were observed. A relationship between the function of alumina as an electron acceptor, resulting in decreasing residual carbon contents with increasing amount of alumina, according to Yamaguchi [25], was confirmed. The optimization of the drying conditions and mix formulations led to an approximately 30% higher cold crushing strength in comparison to the state of the art materials currently in use by industry.

Acknowledgements

The authors would like to thank the German Research Foundation (DFG) for supporting these investigations through the Collaborative Research Centre 920 ‘‘Multi-Functional Filters for Metal Melt Filtration - A Contribution towards Zero Defect Materials’’, Subproject A01.

References

[1] D. Janke, K. Raiber, Grundlegende Untersuchungen zur Optimierung der Filtration von Stahlschmelzen. Technische Forschung Stahl, Europäische Kommission, Luxembourg, 1996, ISBN 92-827-6458-3.
[2] H.-J. Bargel, G. Schulze, Eisenwerkstoffe. Werkstoffkunde, Springer-Verlag, Berlin/Heidelberg/New York, 2005, pp. 141–268. ISBN: 3-540-26107-9.
[3] H. Jacobi, The process metallurgy and materials engineering of steel with high purity and cleanness,(Feuerfeste Werkstoffe und Systeme für die Erzeugung hochreiner Stähle), in: Proceedings of XXXVII (Internationales Feuerfest-Kolloquium, Stahl und Eisen Special 1994), 1994, pp. 5–16.
[4] S. Ovtchinnikov, Kontrollierte Erstarrung und Einschlussbildung bei der Desoxidation von hochreinen Stahlschmelzen, TU Bergakademie Freiberg, Diss., 2002.
[5] K. Wasai, K. Mukai, A. Miyanaga, Observation of inclusion in aluminum deoxidized iron, ISIJ International 42 (5) (2002) 459–466.
[6] P. Hammerschmid, D. Janke, Kenntnisstand zur Abscheidung von Einschlüssen beim Filtrieren von Stahlschmelzen, Stahl und Eisen 108 (5) (1988) 211–219.
[7] P. Hammerschmid, K. Raiber, D. Janke, Abscheidung von Tonerdeeinschlüssen aus Stahl- und Nickel-Basis-Schmelzen mit keramischen Filtern. Stahl und Eisen, Special 1994, Konferenz-Einzelbericht, 1994, 58–64.
[8] O. Davila-Maldonaldo, et al., Simulation of fluid and inclusions dynamics during filtration operations of ductile iron melts using foam filters, Metallurgical and Materials Transactions B 39 (6) (2008) 818–839.
[9] A. Adams, T. Tackaberry, Ceramic filters for ductile iron filtration—your last chance to trap inclusions, Ductile Iron News 3 (1994) 3–8.
[10] E.I. Mogilevskii, V.I. Burtsev, Production technology and tests of ceramic filters for refining precision alloys, Refractories and Industrial Ceramics 41 (2000) 28–30.
[11] H. Jaunich, B. Pech, C. Aneziris, Vorsprung durch Innovation bei der Entwicklung von Speisern und Filter für die Gießereitechnik. cfi-Bericht DKG 80 No. 5, 2003.
[12] J. Luyten, et al., Different methods to synthesize ceramic foams, Journal of the European Ceramic Society 29 (2009) 829–832.
[13] K. Schwartzwalder, Method of making porous ceramic articles, Patent US 3,090,094 (1963).
[14] J. Saggio-Woyansky, C.E. Scott, Processing of porous ceramics, American Ceramic Society Bulletin 71 (11) (1992) 1674–1682.
[15] J. Adler, G. Standke, Offenzellige Schaumkeramik, Teil 2, Keramische Zeitschrift 55 (10) (2003).
[16] C.G. Aneziris, A. Ansorge, H. Jaunich, New approaches of carbon bonded foam filters for filtration of large castings. cfi-Bericht DKG 85 No. 10, 2008.
[17] M. Hasterok, et al., Processing of ceramic preforms for TRIP-matrix-composites, Steel Research International 82 (9) (2011) 1032–1039.
[18] H.O. Pierson, Handbook of Carbon, Graphite, Diamond and Fullerenes, WILEY-VCH Verlag GmbH & Co. KGaA, Weinheim, New Jersey, 1993, ISBN: 0-8155-1339-9.
[19] G. Stephani, et al., Iron based cellular structures—status and prospects, Advanced Engineering Materials 9 (2006) 847–852.
[20] C.G. Aneziris, M. Emmel, Verfahren zur Herstellung kohlenstoffhaltiger und/oder kohlenstoffgebundener keramischer Metallschmelze-Filter, Patent application DE 10 2011 109 682.9 (2011).
[21] C.G. Aneziris, et al., Functional refractory material design for advanced thermal shock performance due to titania additions, Int. J. Appl. Ceram. Technol. 4 (6) (2007) 481–489.
[22] A. Ansorge et al., Patent DE 000060101793 T3 (2008).
[23] C.A. Rottmair, Einfluss der thermischen Prozessführung auf die Eigenschaften von Graphitformteilen, hergestellt durch Pulverspritzguss von Mesophasen-Kohlenstoff, Universität Erlangen-Nürnberg, Diss. (2007).
[24] U. Fischer, Optimierte Auftragsverfahren in der Spritzglasiertechnologie, Freiberger Forschungshefte A897, Freiberg, 2009. ISBN 978-3-86012-368-3.
[25] A. Yamaguchi, Effect of refractory oxides on the oxidation of graphite and amorphous carbon, Journal of the American Ceramic Society 79 (9) (1996) 51.